Supporting Information

A Combined Experimental and Theoretical Approach Revealing Direct Mechanism for Bifunctional Water Splitting on Doped Copper Phosphide

Indranil Mondal*[a], Arup Mahata*[b,c], Heeyoung Kim[d], Ujjwal Pal[e], Filippo De Angelis*[b,f], Jeong Y. Park* [a,d]

[a] *Center for Nanomaterials and Chemical Reactions, Institute for Basic Science (IBS), Daejeon 34141, Republic of Korea*
[b] *Computational Laboratory for Hybrid/Organic Photovoltaics (CLHYO), Istituto CNR di Scienze e Tecnologie Chimiche "Giulio Natta" (CNR-SCITEC), Via Elce di Sotto 8, 06123 Perugia, Italy*
[c] *CompuNet, Istituto Italiano di Tecnologia, Via Morego 30, 16163 Genova, Italy*
[d] *Department of Chemistry, Korea Advanced Institute of Science and Technology (KAIST), Daejeon, 34141, Republic of Korea*
[e] *Department of Energy and Environmental Engineering, CSIR-Indian Institute of Chemical Technology, Hyderabad 500007, India.*
[f] *Department of Chemistry, Biology and Biotechnology, University of Perugia, Via Elce di Sotto 8, 06123 Perugia, Italy*

Content

Computational Details:

First principles calculations were carried out using the projector-augmented wave (PAW)[S1] method, as employed in the Vienna Ab initio Simulation Package (VASP).[S2] The generalized gradient approximation of Perdew-Burke-Ernzerhof (GGA-PBE)[S3,S4] was used for describing the exchange-correlation potential. A plane wave basis set was used for an energy cut-off of 470 eV. The energy criteria for self-consistent calculations were set to 10^{-4} eV between two successive steps, and the atomic forces of all the systems were set to less than 0.01 eV$Å^{-1}$ without any symmetry constraints. Only ions were relaxed for the bulk calculations with experimental cell parameters, whereas both ions and cell parameters were relaxed for slab calculations. A vacuum of ~15 Å was employed in the *z*-directions to avoid interactions between the periodic layers. Slab calculations were carried out in a 2×2 supercell geometry in the periodic *xy*-plane, and the Brillouin zone of the supercell was sampled with a set of 3×3×1 Gamma centered k-point grids for geometry optimization. Symmetric slabs were constructed across the vacuum direction considering 144 and 120 atoms for Cu- and CuP-terminations, respectively. We used 6×6×6 Gamma centered k-point grids for density of state calculations of the bulk structures. Spin polarized calculations were performed for the calculations of Fe-doped systems.

Surface energy of the slabs (E_{sur}) was calculated using the following equation:

$$E_{sur} = (E_{slab} - E_{bulk})/A_{slab}$$

where E_{slab} is the total energy of the pristine/Fe-doped slabs, E_{bulk} is the total energy of the bulk systems containing the same number of atoms in the slabs, and A_{slab} is the total surface area of the slabs.

We constructed both Cu-terminated and CuP-terminated surfaces. Based on the calculated surface energy, the CuP-terminated surface is more stable (Table S4); therefore, we studied the adsorption behavior of the reaction intermediates utilizing the CuP-terminated surface.

The adsorption energies (E_{ad}) of all the possible intermediates were calculated using the following equation:

$$E_{ad} = E_{slab\text{-}adsorbate} - (E_{slab} + E_{adsorbate})$$

where $E_{slab\text{-}adsorbate}$ represents the total energy of the surface with adsorbed species, E_{slab} and $E_{adsorbate}$ represent the total energy of the periodic surface and adsorbed intermediates (*O, *OH, *OOH and *H), respectively.

The ΔZPE correction for adsorbed intermediates was taken from the vibrational frequency calculation by density functional perturbation theory (DFPT). This was done using a selective dynamics approach, where the coordinates of Cu_3P slab atoms were frozen during the frequency calculations. Furthermore, we did not consider the entropy (ΔS) contribution, as it is negligible for adsorbed intermediates.[S5] The ΔS values for the free gaseous molecules were taken from the NIST database.[S6] As the GGA-DFT method cannot accurately calculate the O_2 bond energy, we took the O_2 bond energy associated with water formation ($2H_2+O_2=2H_2O$), which is 4.92 eV.[S5,S7,S8] ΔG_{pH} is the correction of the H^+ free energy and depends on whether the reaction under acidic or basic condition. $\Delta G_{pH} = - k_B T \ln[H^+] = pH \times k_B T \ln 10$, where k_B is the Boltzmann constant, T is the temperature and pH is equal to 14 for alkaline medium. The free energy of OH^- was derived as $G_{OH-} = G_{H2O(l)} - G_{H+}$. The free energy for gas phase water is calculated at 0.035 bars, because this is the equilibrium pressure in contact with liquid water at 298 K. At these conditions, the free energy of gas phase water is equal to the free energy of liquid water.[S9]

Materials Characterization:

Wide-angle X-ray diffraction patterns were collected using a multipurpose attachment from SmartLab, RIGAKU. The measurements were taken at a 2θ scan range of 10–90°, scan speed of 2.4°/min, and step size of 0.01 Å, using CuK_α radiation to identify the phases. The exterior morphology, elemental mapping and EDXS were analyzed using a Magellan 400 scanning electron microscope (SEM). Transmission electron microscopy (TEM) was carried out using field emission transmission electron microscopy (FE-TEM; Tecnai TF30 ST). The TEM samples were prepared by drop casting the ethanol suspension of each respective catalyst on a 300-mesh copper grid. X-ray photoelectron spectroscopy (XPS) was carried out using a Thermo VG Scientific Sigma Probe system equipped with an Al-Kα X-ray source (1486.3 eV) with an energy resolution of 0.47 eV full width at half maximum under ultrahigh vacuum conditions of 10^{-10} Torr. FM40 Contact Angle Measuring Instrument Easydrop was used to measure the contact angle on carbon fiber surface. A Monochrome interline CCD, 25/30 fps, 752×582 px camera was used during analysis.

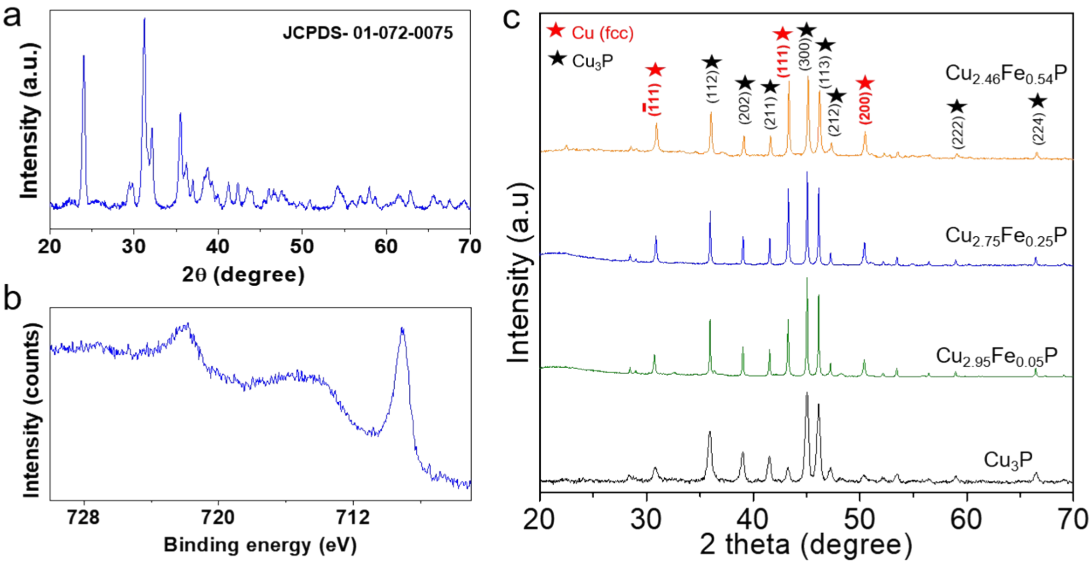

Fig. S1. (a) Wide-angle powder XRD pattern of post hydrothermal product which is isolated as pure malachite (precursor for Fe doped Cu_3P) (b) Fe 2p XPS profile of post hydrothermal product and (c) wide-angle XRD pattern of different electrocatalysts prepared with different Fe doping.

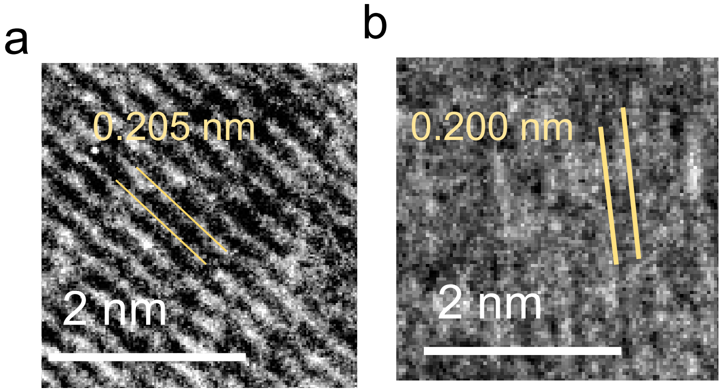

Fig. S2 HRTEM shows the (110) plane lattice spacing of (a) Cu_3P and (b) Fe-doped Cu_3P.

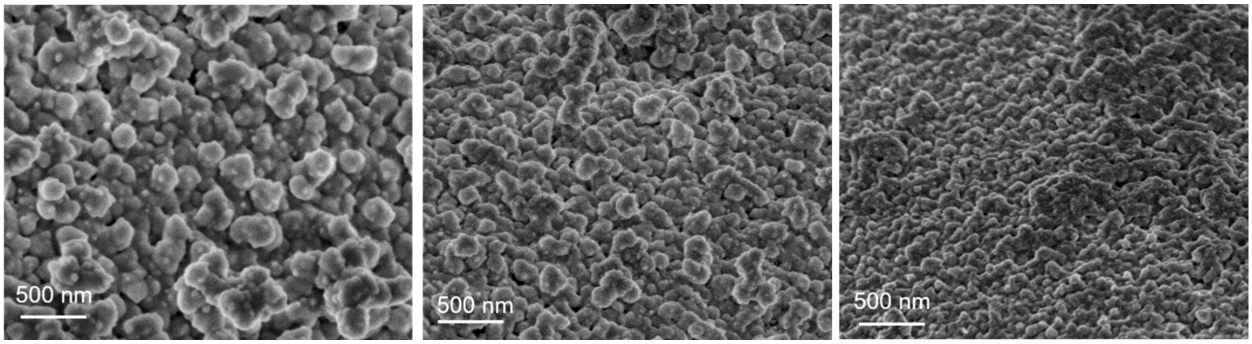

Fig. S3. SEM images of the (a) $Cu_{2.95}F_{0.05}P$ (b) $Cu_{2.75}F_{0.25}P$ and (c) $Cu_{2.46}F_{0.54}P$. It clearly shows that the size of the nanocucurbits decrease with increased Fe dosing amount, resulting in a more hydrophilic surface.

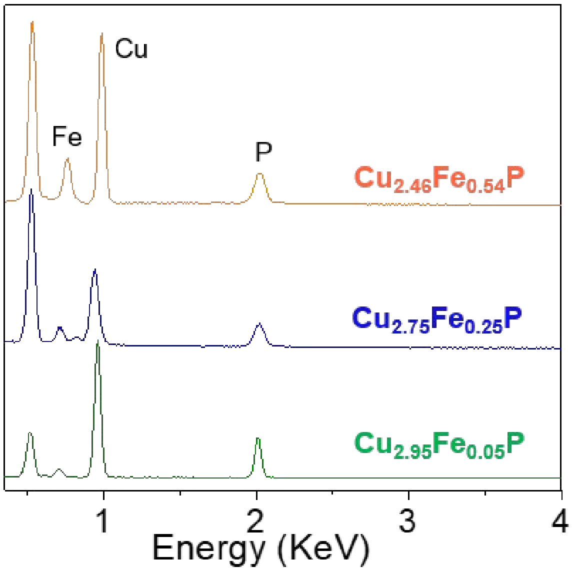

Fig. S4. SEM-EDX spectra of various Fe doped Cu_3P catalysts. Based on the atomic percentage, the empirical formula was presented.

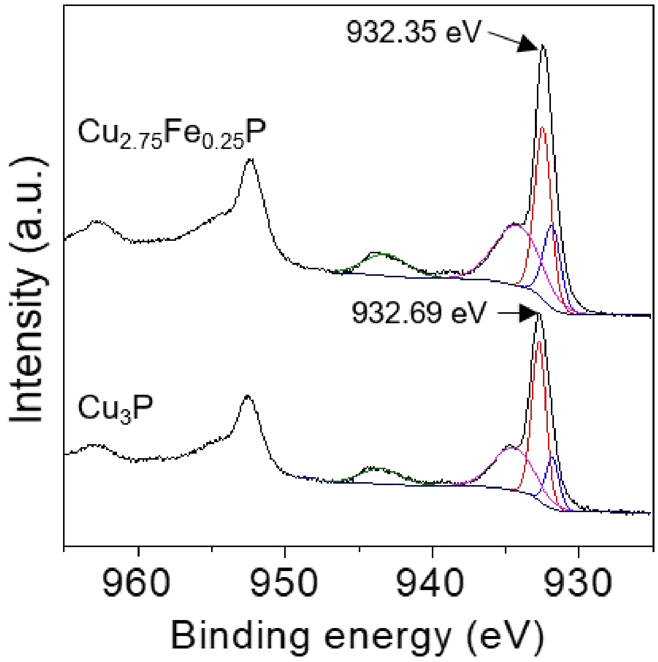

Fig. S5. Cu 2p XPS spectra of pristine and Fe doped Cu_3P ($Cu_{2.75}F_{0.25}P$)

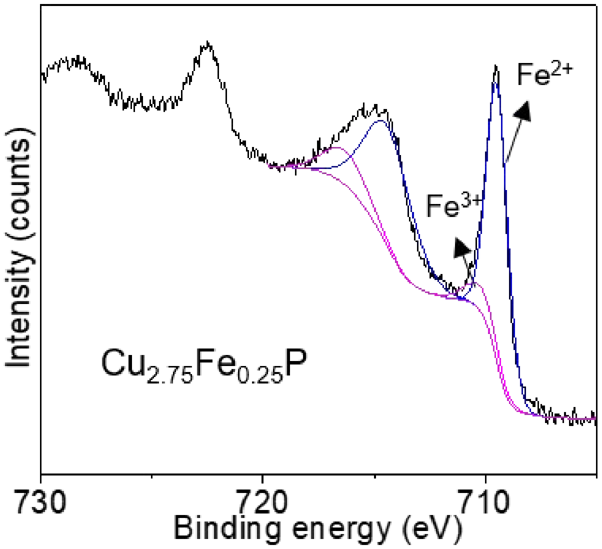

Fig. S6. Fe 2p XPS profile of Fe doped Cu_3P ($Cu_{2.75}Fe_{0.25}P$).

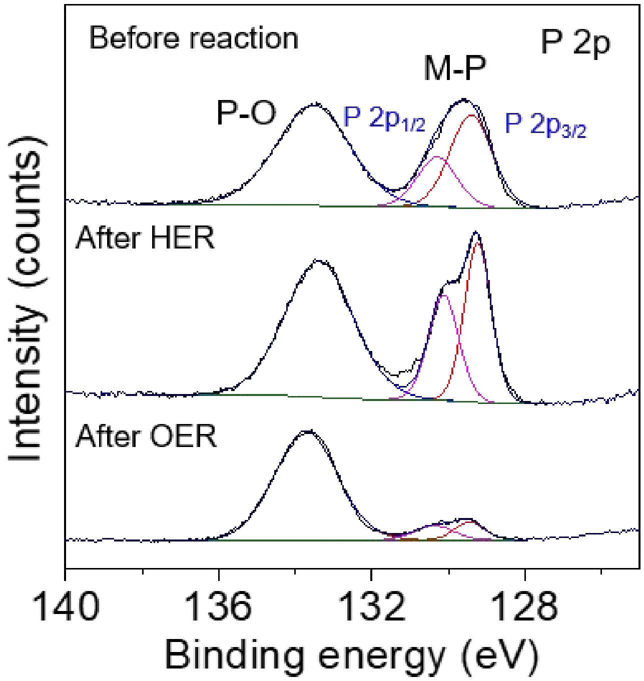

Fig. S7. P 2p XPS profile of $Cu_{2.75}Fe_{0.25}P$ at different stages of the reaction.

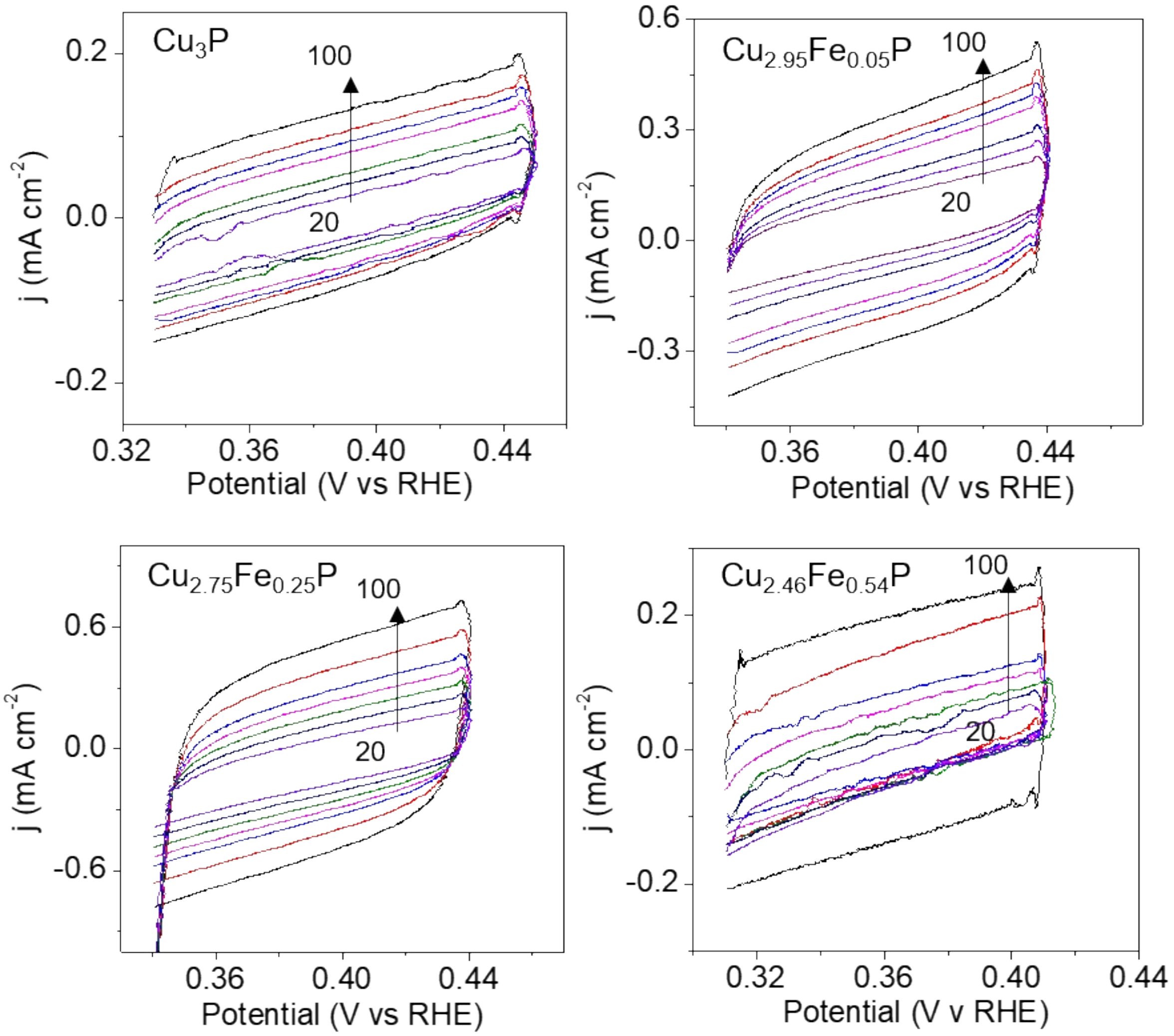

Fig. S8. Cyclic voltammograms recorded for the doped and undoped Cu_3P within a non-faradaic region at various scan rates (mVs^{-1}) for determining the double layer capacitance. The total output current can be expressed as $J = J_f + C_{dl}$ (dE/dt), where J_f represents the Faradaic current, C_{dl} is double layer capacitance, (dE/dt) is scan rate. At non-faradaic zone, from the difference of anodic and cathodic current density with the function of scan rate resulted a linear curve. The determination of the slope value corresponds to the C_{dl} of the respective electrode. The linear curve and the slope value is mentioned in manuscript (Fig. 3c). The C_{dl} of each electrode serves as an estimate of the effective electrochemically active surface area of the solid–liquid interface. The calculated C_{dl} values for the Cu_3P, $Cu_{2.95}Fe_{0.05}P$, $Cu_{2.75}Fe_{0.25}P$, $Cu_{2.46}Fe_{0.54}P$ is 1.2 μF cm^{-2}, 1.4 μF cm^{-2}, 5 μF cm^{-2}, and 3.1 μF cm^{-2} respectively.

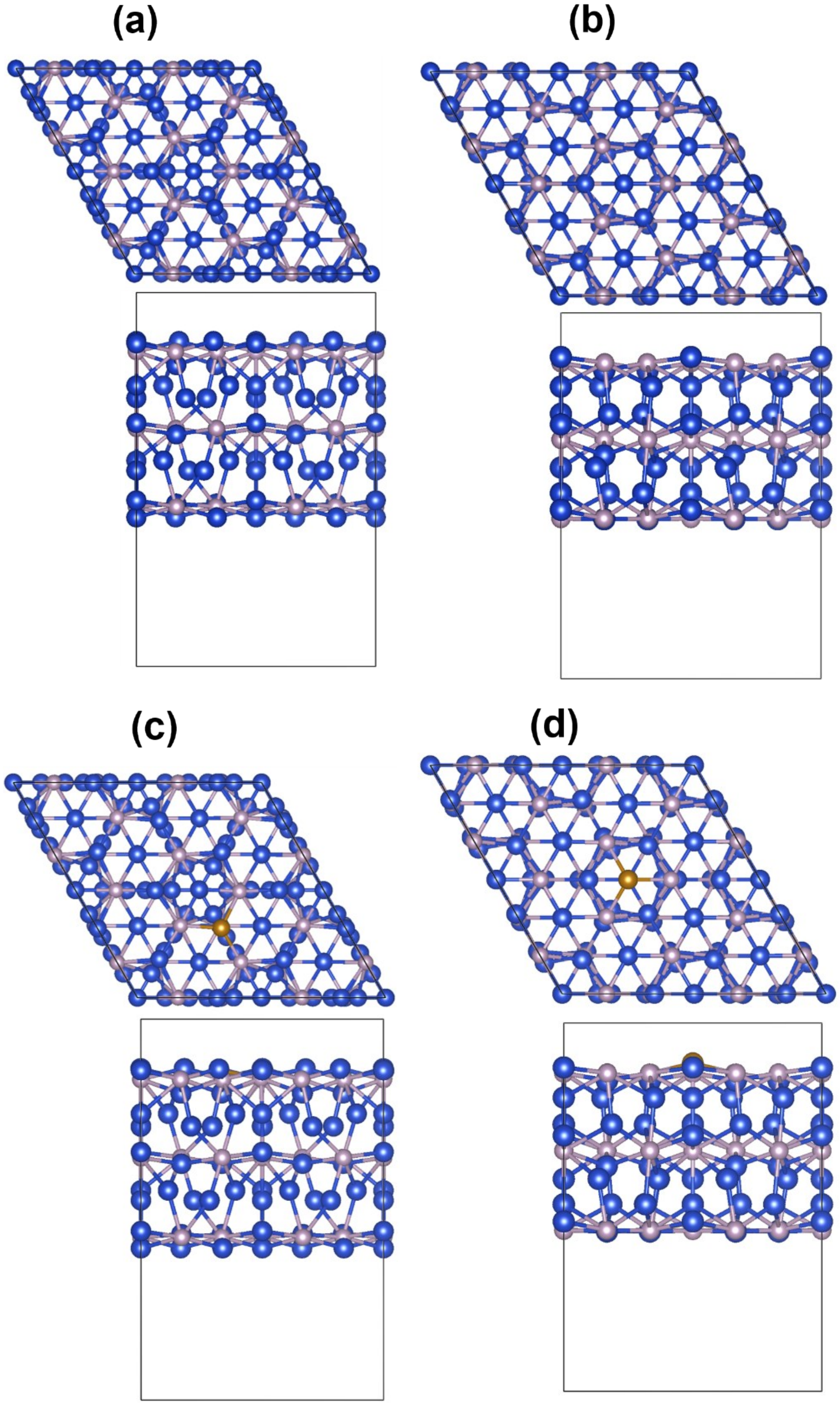

Fig. S9. Optimized structures for the (0001) slabs of (a) Cu-ter, (b) CuP-ter, (c) CuFe-ter and (d) CuFeP-ter

Table S1. Crystal cell parameter measured using wide angle XRD.

Catalyst	Cell parameter	Angles	Reitveld refinement parameter	% of Cu phase
Cu_3P	a = b= 6.9593 and c = 7.143	α = β= 90° γ = 120 °	R_w is 10.52% (sigma 1.55)	16.4%
$Cu_{2.75}Fe_{0.25}P$	a = b= 6.9581 and c = 7.140	α = β= 90° γ = 120 °	R_w is 7.14% (sigma 1.16)	43.2%

Table S2. Amount of Fe content after doping in Cu_3P.

Theoretical (mol%/wt%)	ICP-AES (wt%)	SEM EDSX (wt%/atomic composition)
2/1.8	1.5 ± 0.05	1.6 ± 0.05 ($Cu_{2.95}Fe_{0.05}P$)
10/8.9	7.4 ± 0.1	7.9 ± 0.05 ($Cu_{2.75}Fe_{0.25}P$)
20/19	17.6 ± 0.3	16.5 ± 0.05 ($Cu_{2.46}Fe_{0.54}P$)

Table S3. Surface Energy (meV/Å^2) for the different terminations

Systems	**Pristine**	**Fe-doped**
Cu/Fe-terminated	25	26
CuP/FeP-terminated	3	6

Table S4. Adsorption energies (eV) for all the possible adsorption intermediates in pristine and Fe-doped surfaces

Reaction intermediates	**Pristine**	**Fe-doped**
*O (Cu-P bridge)	-4.40	-4.45
*O (Fe-P bridge)	-	-4.89
*O (Cu-top)	-2.09	-3.95
*O (Fe-top)	-	-4.55
*O (P-top)	-4.28	Not stable. Move to bridge site
*O (fcc)	Not stable. Move to bridge site	Not stable. Move to bridge site
*OH (Cu-P bridge)	-2.31	-2.09
*OH (Fe-P bridge)	-	-2.41
*OH (Cu-top)	-1.92	-1.62
*OH (Fe-top)	-	-3.02
*OH (P-top)	-2.39	-2.35
*OOH (Cu-P bridge)	-2.93	Not stable. Move to top site
*OOH (Fe-P bridge)	-	Not stable. Move to top site
*OOH (Cu top)	-2.86	-2.77
*OOH (Fe top)	-	-3.93
*OOH (P top)	-3.13	-3.00
*H (Cu-P bridge)	-2.05	-1.68

*H (Fe-P bridge)	-	-1.57
*H (Cu top)	-1.52	-1.50
*H (Fe top)	-	-2.23
*H (P top)	-2.18	-1.35

Table S5 Activity comparison among different earth abundant bifunctional catalyst for overall water splitting.

Sl No	**Catalyst**	**Electrolyte/process**	**Current density/potential**	**Catalyst amount**	**Reference**
1.	Ordered CoMn/N doped C superlattice structure	1 M KOH/OWS	100 mA cm-2 at 1.78 V of cell voltage	2.0 mg·cm^{-2}	*J. Am. Chem. Soc.*, 2015, **137**, 14305−14312
2.	Carbon Nanotube-Supported $MoSe_2$ Holey Flake:Mo_2C Ball Hybrids	1 M KOH/bifunctional	0.089 V and 0.241 V for HER and OER respectively	0.2 mg cm^{-2}.	*ACS Nano*, 2019, **13**, 3162−3176
3.	NiFePS on nickel foam	1.0 M KOH/OWS	50 mA cm^{-2} at 1.9 V	-----	*ACS Nano*, 2017, **11**, 10303−10312
4.	Epitaxial Dinickel Phosphide to 2D Nickel thiophosphate	1.0 M KOH/OWS	100 mA cm^{-2} at 1.74 V of cell voltage	1.0 mg cm-^{2}	*ACS Nano*, 2019, **13**, 7975−7984
5.	NiSe Nanowire Film Supported on Nickel Foam	1.0 M KOH/OWS	50 mA cm^{-2} at 1.9 V of cell voltage	2.8 mg cm^{-2}	*Angew. Chem. Int. Ed.*, 2015, **54**, 9351–9355
6.	MoS_2/Ni_3S_2 Heterostructures	1.0 M KOH/OWS	10 mA cm^{-2} at 1.56 V of cell voltage	3 mg cm^{-2}	*Angew. Chem. Int. Ed.*, 2016, **55**, 6702–6707
7.	High-Index Faceted Ni_3S_2 Nanosheet on nickel foam	1 M NaOH/OWS	20 mA cm^{-2} at 1.53 V of cell voltage	1.6 mg cm^{-2}	*J. Am. Chem. Soc.*, 2015, **137**, 14023−14026
8.	Nitrogen-doped tungsten carbide nanoarray	1 M H_2SO_4/OWS	20 mA cm^{-2} at 1.65 V of cell voltage	10 mg cm^{-2}	*Nat. Commun.*, 2018, 9, 924
9.	Cu nanowires shelled with NiFe layered double hydroxide	1 M KOH/OWS	100 mA cm^{-2} at 1.7 V of cell voltage	2.2 mg cm^{-2}	*Energy Environ. Sci.*, 2017, **10**, 1820-1827

10.	Ultrathin Feroxyhyte Nanosheets	1.0 M KOH/OWS	100 mA cm^{-2} at 1.94 V of cell voltage	0.16 mg cm^{-2}	*Adv. Mater.*, 2018, **30**, 1803144
11.	Co_3O_4@3D Ti_3C_2-MXene	1 M KOH/OWS	100 mA cm^{-2} at 1.65 V of cell voltage	0.4 mg cm^{-2}	*ACS Nano*, 2018, **12**, 8017−8028
12.	Cu_9S_5/NF	1 M KOH/OER	100 mA cm^{-2} at 1.6 V (vs RHE)	0.6 mg cm^{-2}	*Chem.: Asia. J.*, 2020, **15**, 852-859.
13.	CuSe/NF	1 M KOH/OWS	10 mA cm^{-2} at 1.72 V of cell voltage	--	*ChemSusChem*, 2020, **13**, 3222-3229

References

[S1] P. E. Blochl, *Phys. Rev. B*, 1994, **50**, 17953–17979.

[S2] G. Kresse, J. Furthmuller, *Phys. Rev. B*, 1996, **54**, 11169–11186.

[S3] J. P. Perdew, K. Burke, M. Ernzerhof, *Phys. Rev. Lett*., 1996, **77**, 3865–3868.

[S4] J. P. Perdew, J. A. Chevary, S. H. Vosko, C. Fiolhais, *Phys. Rev. B*, 1992, **46**, 6671–6687.

[S5] K. Nørskov, J. Rossmeisl, A. Logadottir, L. Lindqvist, J. R. Kitchin, T. Bligaard, H. Jónsson, *J. Phys. Chem. B*, 2004, **108**, 17886–17892.

[S6] Computational Chemistry Comparison and Benchmark Database, Standard Reference Database 101, National Institute of Standards and Technology

[S7] D. Shin, S. Sinthika, M. Choi, R. Thapa, N. Park, *ACS Catal*., 2014, **4**, 4074–4080.

[S8] D. Shin, R. Thapa, N. Park, Curr. *Appl. Phys*., 2015, **15**, 727–732.

[S9] Xu, D. Chen, D. Cao, X. C. Zeng, *Nat. Catal.*, 2018, **1**, 339–348.